Journal of Dispersion Science and Technology

ISSN: 0193-2691 (Print) 1532-2351 (Online) Journal homepage: http://www.tandfonline.com/loi/ldis20

Using molecular dynamics simulations to identify the key factors responsible for chiral recognition by an amino acid-based molecular micelle

Kevin F. Morris, Eugene J. Billiot, Fereshteh H. Billiot, Jordan A. Ingle, Kevin B. Krause, Corbin R. Lewis, Kenny B. Lipkowitz, William M. Southerland & Yayin Fang

To cite this article: Kevin F. Morris, Eugene J. Billiot, Fereshteh H. Billiot, Jordan A. Ingle, Kevin B. Krause, Corbin R. Lewis, Kenny B. Lipkowitz, William M. Southerland & Yayin Fang (2018): Using molecular dynamics simulations to identify the key factors responsible for chiral recognition by an amino acid-based molecular micelle, Journal of Dispersion Science and Technology, DOI: 10.1080/01932691.2018.1479267

To link to this article: https://doi.org/10.1080/01932691.2018.1479267

JOURNAL OF DISPERSION SCIENCE AND TECHNOLOGY
https://doi.org/10.1080/01932691.2018.1479267

Using molecular dynamics simulations to identify the key factors responsible for chiral recognition by an amino acid-based molecular micelle

Kevin F. Morris[a], Eugene J. Billiot[b], Fereshteh H. Billiot[b], Jordan A. Ingle[a], Kevin B. Krause[a], Corbin R. Lewis[b], Kenny B. Lipkowitz[c], William M. Southerland[d], and Yayin Fang[d]

[a]Department of Chemistry, Carthage College, Kenosha, WI, USA; [b]Department of Physical and Environmental Sciences, Texas A&M University-Corpus Christi, Corpus Christi, TX, USA; [c]Office of Naval Research, Arlington, VA, USA; [d]Department of Biochemistry and Molecular Biology, Howard University College of Medicine, Howard University, Washington, DC, USA

ABSTRACT

Molecular dynamics (MD) simulations were used to investigate the binding of six chiral compounds to the amino acid-based molecular micelle (MM) poly-(sodium undecyl-(L)-leucine-leucine) or poly(SULL). The MM investigated is used as a chiral selector in capillary electrophoresis. The project goal was to characterize the chiral recognition mechanism in these separations and to move toward predictive models to identify the best amino acid-based MM for a given separation. Poly(SULL) was found to contain six binding sites into which chiral compounds could insert. Four sites had similar sizes, shapes, and electrostatic properties. Enantiomers of alprenolol, propranolol, 1,1′-bi-2-naphthyl-2,2′-diyl hydrogen phosphate, 1,1′-bi-2-naphthol, chlorthalidone, or lorazepam were separately docked into each binding pocket and MD simulations with the resulting intermolecular complexes were performed. Solvent-accessible surface area calculations showed the compounds preferentially associated with binding sites where they penetrated into the MM core and shielded their non-polar atoms from solvent. Furthermore, with five of the six compounds the enantiomer with the most favorable free energy of MM association also experienced the most favorable intermolecular hydrogen bonding interactions with the MM. This result suggests that stereoselective intermolecular hydrogen bonds play an important role in chiral discrimination in separations using amino acid-based MMs.

GRAPHICAL ABSTRACT

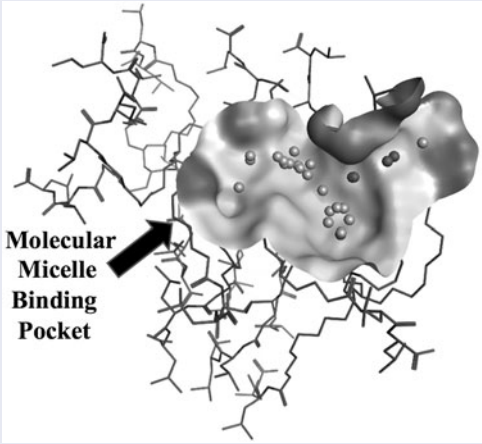

ARTICLE HISTORY
Received 2 April 2018
Accepted 16 May 2018

KEYWORDS
Amino acid-based surfactant; chiral separations; molecular dynamics simulation; molecular micelle

Introduction

The enantiomers of chiral drugs often have different potencies, toxicities, and biochemical properties. For example, the L-enantiomer of dopamine calms tremors, whereas the D-enantiomer is toxic to nerve cells.[1,2] Therefore, the FDA and other worldwide regulatory agencies require manufactures to test and prove the enantiomeric purity of chiral drugs.[3] This requirement has led to the development of many chiral chromatographic techniques using thin layer

CONTACT Yayin Fang yfang@howard.edu Department of Biochemistry and Molecular Biology, Howard University College of Medicine, Howard University, 520 W Street NW, Washington, DC 20059, USA.

Supplemental data for this article can be accessed on the publisher's website.

chromatography, gas chromatography, high-performance liquid chromatography, and capillary electrophoresis (CE)-based methods.[4,5] In each of these techniques, (R) and (S) enantiomers in a racemic mixture are separated based upon the often small differences in their interactions with other chiral molecules making up the chromatographic stationary or pseudostationary phases.

In chiral CE, the enantiomers in a racemic mixture and a chiral selector are pulled down a capillary by an electric field.[6] Examples of chiral selectors include micelles, crown ethers, polysaccharides, polymers, and cyclodextrins.[7] The enantiomers are separated when they interact differentially with these chiral selectors. Recent developments in chiral CE separations have been reviewed by Sciba.[7] CE-based chiral separations, when compared to gas and liquid chromatography, often have lower operating costs, smaller sample size requirements, shorter analysis times, and higher separation efficiencies.[8]

The class of CE selectors investigated here are amino acid-based chiral molecular micelles (MM). These selectors were first applied in CE separations in the 1990s[9,10] and have since been used to separate enantiomers of a wide range of chiral compounds.[11–22] Amino acid-based MMs are polymeric materials containing surfactant monomers like those shown in Figure 1a with a hydrocarbon tail attached to an amino acid or dipeptide headgroup. Also as shown in Figure 1a, MMs are formed when a polymerization reaction is carried out and the monomers are covalently linked to one another with covalent bonds at the end of each surfactant's hydrocarbon tail. MMs as depicted in Figure 1a, therefore have a single macromolecular structure with a chiral, hydrophilic surface, and a non-polar hydrocarbon core.[23] In CE separations, covalently linking the surfactant molecules eliminates the surfactants' critical micelle concentration, allows MMs to be used in lower concentrations than conventional micelles, and often increases chiral resolution.[11,12]

The amino acids in a MM's dipeptide headgroup and the order in which the amino acids are connected have a dramatic effect on chiral resolution in CE separations.[8,12,13] Therefore, analysts must often decide which headgroup is likely to be the most effective chiral selector for the separation problem at hand. The long-term goal of this project is to build a set of molecular modeling-based predictive models that will identify the most effective chiral selector for a given separation problem. Reliable predictive models, however, must be based upon criteria that come from an understanding of the chiral recognition mechanism. This mechanism has been previously investigated by examining how chiral compounds bind to a MM with two different amino acids, leucine and valine, in the dipeptide headgroup.[24–28] In this investigation, molecular dynamics (MD) simulations were used to further probe this mechanism by studying how six chiral compounds interacted with the MM poly-(sodium undecyl-(L)-leucine-leucine) or poly(SULL). The structure of this MM is shown in Figure 1a. Note that there are two identical leucine amino acids in the dipeptide headgroup. Poly(SULL) was also chosen because results from the MD simulations could be compared to those from literature CE experiments in which poly(SULL) was used as the chiral selector.[22]

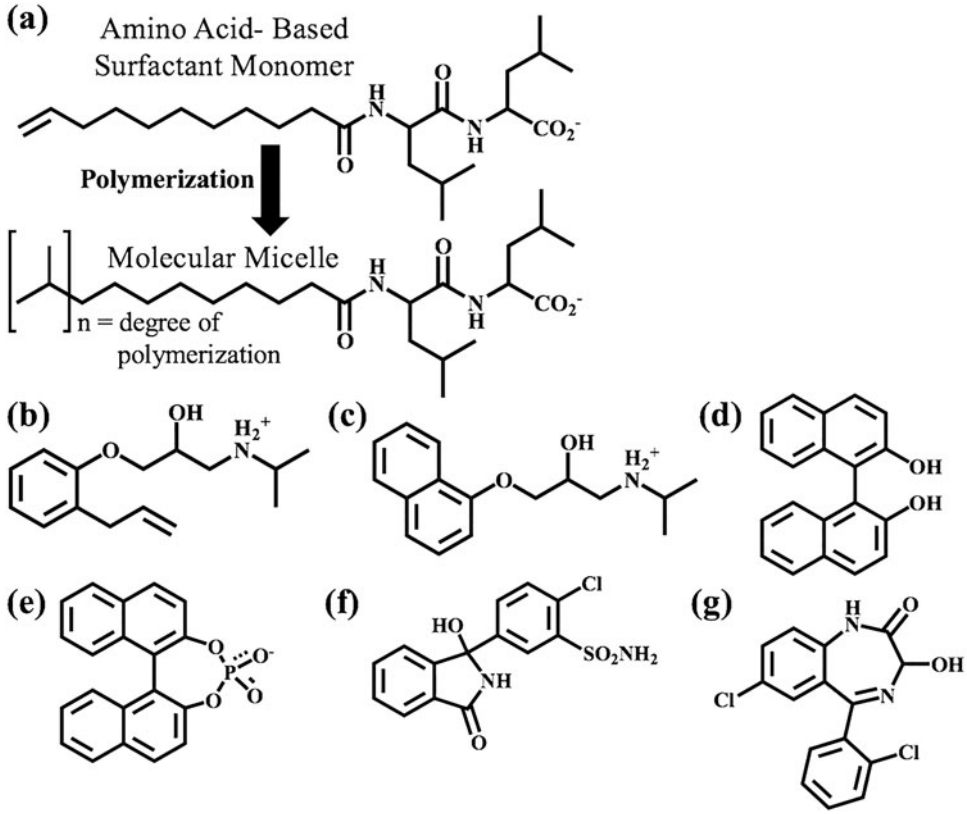

Figure 1. Chemical structures of (a) poly-(sodium undecyl-(L)-leucine-leucine), (b) alprenolol, (c) propranolol, (d) 1,1′-bi-2-naphthol, (e) 1,1′-binaphthyl-2,2′-diyl hydrogen phosphate, (f) chlorthalidone, (g) lorazepam.

The ligands investigated in this study were alprenolol, propranolol, 1,1′-bi-2-naphthyl-2,2′-diyl hydrogen phosphate (BNP), 1,1′-bi-2-naphthol (BOH), chlorthalidone, and lorazepam. The structures of these compounds are shown in Figure 1b–1g. The binding of alprenolol, propranolol, BOH, and BNP enantiomers to poly(SULL) have been investigated experimentally by Billiot et al.[22] Propranolol and alprenolol are β-blocker drugs and chlorthalidone is a thiazide diuretic used to treat fluid retention in patients with hypertension.[29] BNP and BOH are used in chiral syntheses[30,31] and their interactions with amino acid-based MM have been studied by a variety of experimental techniques.[32–37] Finally, lorazepam is a benzodiazepine drug used to treat anxiety, insomnia, and seizures.[38] By investigating the association of these structurally diverse chiral compounds with poly(SULL), the MM binding sites with the most favorable ligand: MM intermolecular interactions were identified along with the factors determining which of a chiral compound's enantiomers had the lower MM binding-free energy. The insight gained will then be used in subsequent work to build the quantitative predictive models discussed above.

Experimental details

MD simulations and ligand docking

The molecular modeling and MD simulation methods used in this project are described in detail in references.[26,27] The Supplemental Information section of reference[27] also contains the input files used to carry out the MD simulations. The methods used are summarized as follows. First, a poly(SULL) micelle was built by connecting together 19 SULL surfactant monomer chains with covalent bonds at the end of each monomer's hydrocarbon tail. Fluorescence quenching experiments have shown that poly(SULL) contains on average 19 surfactant monomers.[23] The monomers were connected in this fashion in a manner consistent with our previous work and because the CE chiral selectors under investigation contain covalent bonds connecting the individual surfactant monomers.[24–28] AMBER 14 was then used to carry out a 60.0 ns MD simulation on a system containing the poly(SULL) molecule, 19 sodium counter-ions and ≈8000 TIP3P water molecules.[39] The average poly(SULL) structure was then calculated. Next, the root mean squared deviation (RMSD) of each MD simulation structure with respect to the average structure was determined. A representative poly(SULL) structure having a low RMSD with respect to the average structure was then extracted from the MD simulation. This method was employed to choose a specific structure from the MD simulation that was most similar to the average structure. This representative poly(SULL) structure was then used in the ligand docking analyses.[26–28]

The *MOE* (Molecular Operating Environment, Chemical Computing Group, Inc., Montreal, Canada) software package was used to identify ligand binding sites within the poly(SULL) micelle and to dock ligand enantiomers into each binding pocket.[40] The ligands were docked into the binding pockets identified by *MOE* because CE experiments have shown that the ligands investigated and other compounds with similar structures do in fact associate with this MM. Since the association between the ligands and poly(SULL) has been confirmed experimentally, site identification and docking were done to determine exactly where and how the ligands bound to the MM in question. These methods were also employed in our previous studies.[24–28] In the site identification and docking analyses, the representative poly(SULL) structure from above was first imported into *MOE* and the molecule's binding pockets were identified using the Site Finder module. In this step of the analysis, the alpha sphere and discrete-flow methods developed by Edelsbrunner and Mucke[41] and Edelsbrunner and Shah[42] were used. The site finder step identified six different binding pockets at different locations within the poly(SULL) molecule. *MOE* also placed alpha spheres within each binding pocket to characterize its electrostatic properties. An alpha sphere in *MOE* is a dummy atom with four receptor atoms on its boundary.[41,42] The alpha spheres found within each binding site were colored white if they were in a non-polar or poor hydrogen bonding region of the pocket. Alpha spheres were colored red if they were in a polar pocket region where hydrogen bonding could occur. The relative numbers of white and red alpha spheres within a given pocket were used to assess whether the pocket provided ligand enantiomers with a primarily hydrophobic or hydrophilic environment.

After the binding pockets were identified, *MOE* was then used to separately dock either the (R) or (S) enantiomer of each ligand investigated into each of the six different poly(SULL) binding pockets. The poly(SULL) receptor was rigid and each ligand enantiomer was completely flexible during the docking analysis. Hundreds of ligand poses were examined. Each pose was also given a score based upon the free energy of the ligand:receptor complex. Scoring was done using dG scoring function developed by Dal Ben et al.[43] The highest scoring pose or the pose with the lowest free energy was used in the MD simulation analyses. Since each chiral ligand had two enantiomers and poly(SULL) had six biding pockets, a total of 12 docked structures, that is, either (R) or (S) docked into each of the six MM pockets, was generated for each chiral compound studied.

MD simulations with all of these intermolecular complexes were carried out using AMBER 14 and the parm99 force field.[39,44] The system used for each MD simulation contained the poly(SULL):enantiomer complex of interest, 19 sodium counterions, and ≈8000 TIP3P water molecules. An energy minimization step was performed first followed by a 20 picoseconds MD simulation to warm the system to 300 K. A 1 ns MD simulation was then used to equilibrate to a pressure of one atmosphere before the 60.0 ns MD simulation production run was carried out. In the production run, the time step was 2 fs, structures were stored every 0.2 ps, and cubic periodic boundary conditions were employed.

Binding free energy analyses

MM binding free energy calculations were performed with AMBER 14 using the mm-PBSA method developed by

Kollman et al.[45] The $\Delta G_{binding}$ values calculated with this method correspond to the difference in free energy between each MM:enantiomer complex and the sum of the free energies of the separate MM receptor and ligand enantiomer. These calculations were performed for the (R) and (S) enantiomers of each chiral compound binding to all six poly(SULL) binding pockets. The fractional occupancies of each MM binding pocket were calculated as well. These values correspond to the fraction of time that the ligand will bind to each poly(SULL) pocket, based upon the calculated free energies of binding. Fractional occupancies were calculated with Equation (1).[26]

$$f_i = \frac{e^{-G_i/k_B \cdot T}}{\sum_{i=1}^{N} e^{-G_i/k_B \cdot T}} \quad [1]$$

G_i is the binding free energy of one of the ligand enantiomers in the ith pocket of the MM, k_B is Boltzmann's constant, and T is Kelvin temperature. The summation in Equation (1) is over the six poly(SULL) binding sites. In most of the chiral compounds investigated, the f_i values calculated by Equation (1) were near one for one of the MM pockets and near zero for the others. This result indicates that the ligand enantiomers bind almost exclusively to the MM pocket with the large f_i value. Finally, a pocket averaged free energy of binding was also calculated for each ligand enantiomer by multiplying each pocket's respective G_i and f_i values and summing these products over the six binding pockets.[28] Tables 1–3 report $\Delta G_{binding}$ and f_i values for each ligand enantiomer binding to all six poly(SULL) binding pockets. Pocket-averaged binding free energies for each ligand enantiomer are presented as well.

These free energy of binding calculations provide an important link between MD simulation and experimental results. In chiral CE, ligand enantiomers separate based upon their relative free energies of binding to the chiral selector.[36] The enantiomer exhibiting the larger or less favorable free energy of MM binding elutes before the enantiomer with the lower $\Delta G_{binding}$ value.[23,36–38] Therefore, free energy calculations can be used to validate MD simulation methods and to predict elution order in CE separations.[26–28]

Solvent-accessible surface area (SASA) and hydrogen bond analyses

Analyses of the MD simulation trajectories were done using the CPPTRAJ utilities in AMBER 14.[46] For each ligand enantiomer investigated, SASA calculations were carried out to assess the extent to which the ligand enantiomers penetrated into the MM hydrocarbon core. The SASA represents the surface area of the ligand molecule in Å^2 that is exposed or accessible to solvent molecules. An enantiomer found deep within the hydrocarbon core of the MM would be expected to have a low SASA value. The SASA would be higher for a ligand enantiomer binding near the MM surface where it is likely surrounded by more solvent molecules.

The ligands investigated in this study, however, had different molar masses and numbers of atoms. Therefore, a smaller ligand molecule binding nearer the surface of the MM could have a SASA comparable to a larger ligand molecule found deeper within the MM core. In order to facilitate comparison of molecules with different sizes, MD simulations were also carried out with each ligand in free solution with no MM present. The MD simulation average percentage decrease in SASA upon moving from the free solution to the MM-bound states was then calculated for each MM pocket.[28] A large average percentage decreases in SASA for a given pocket, indicates that within that pocket the ligand is able to penetrate deep in the MM core. A smaller average percentage decrease in the SASA is characteristic of a MM pocket that places the ligand nearer the MM surface and closer to the bulk aqueous phase. Tables 1–3 report the percentage decrease in SASA values calculated for each ligand enantiomer binding to all six

Table 1. Free energies of binding, pocket fraction occupied values, and percentage decrease in solvent-accessible surface area for alprenolol and propranolol enantiomers binding to poly(SULL).

	Pocket 1	Pocket 2	Pocket 3	Pocket 4	Pocket 5	Pocket 6
R-Alprenolol						
$\Delta G_{binding}$ (kJ·mol^{-1})	−44.7	−72.9	−75.4	−58.5	−70.3	−72.4
Fraction occupied	–	0.21	0.55	–	0.07	0.17
% SASA decrease	24.7	49.3	54.7	40.7	49.5	49.3
		Pocket average $\Delta G_{binding} = -74.0$ kJ·mol^{-1}				
S-Alprenolol						
$\Delta G_{binding}$ (kJ·mol^{-1})	−86.2	−73.6	−107.5	−83.6	−67.4	−101.0
Fraction occupied	–	–	0.93	–	–	0.07
% SASA decrease	54.2	53.0	69.9	62.4	43.9	59.1
		Pocket average $\Delta G_{binding} = -107.0$ kJ·mol^{-1}				
R-Propranolol						
$\Delta G_{binding}$ (kJ·mol^{-1})	−74.9	−103.2	−62.4	−83.4	−88.2	−75.2
Fraction occupied	–	1.00	–	–	–	–
% SASA decrease	42.7	52.3	40.3	58.3	51.7	8.8
		Pocket average $\Delta G_{binding} = -103.2$ kJ·mol^{-1}				
S-Propranolol						
$\Delta G_{binding}$ (kJ·mol^{-1})	−62.0	−59.8	−86.4	−117.7	−110.3	−57.9
Fraction occupied	–	–	–	0.95	0.05	–
% SASA decrease	42.1	45.3	50.2	67.4	61.9	1.0
		Pocket average $\Delta G_{binding} = -117.3$ kJ·mol^{-1}				

Table 2. Free energies of binding, pocket fraction occupied values, and percentage decrease in solvent-accessible surface area for BOH and BNP enantiomers binding to poly(SULL).

	Pocket 1	Pocket 2	Pocket 3	Pocket 4	Pocket 5	Pocket 6
R-BOH						
$\Delta G_{binding}$ (kJ.mol^{-1})	−56.7	−53.1	−49.4	−58.6	−41.2	−88.1
Fraction occupied	–	–	–	–	–	1.00
% SASA decrease	55.1	59.2	55.9	65.4	1.6	69.5
		Pocket average $\Delta G_{binding} = -88.1$ kJ·mol^{-1}				
S-BOH						
$\Delta G_{binding}$ (kJ.mol^{-1})	−45.1	−39.6	−45.8	−39.8	−39.7	−61.7
Fraction occupied	–	–	–	–	–	1.00
% SASA decrease	46.2	46.6	54.3	41.9	42.4	59.1
		Pocket average $\Delta G_{binding} = -61.6$ kJ·mol^{-1}				
R-BNP						
$\Delta G_{binding}$ (kJ.mol^{-1})	−28.0	−36.8	−46.0	−28.4	−26.3	−25.6
Fraction occupied	–	0.02	0.97	–	–	–
% SASA decrease	50.9	55.4	57.1	42.3	36.3	34.6
		Pocket average $\Delta G_{binding} = -45.7$ kJ·mol^{-1}				
S-BNP						
$\Delta G_{binding}$ (kJ.mol^{-1})	−42.8	−56.8	−66.6	−28.0	−39.2	−51.6
Fraction occupied	–	0.02	0.98	–	–	–
% SASA decrease	53.4	60.6	77.7	37.0	47.0	52.2
		Pocket average $\Delta G_{binding} = -66.4$ kJ·mol^{-1}				

Table 3. Free energies of binding, pocket fraction occupied values, and percentage decrease in solvent-accessible surface area for chlorthalidone and lorazepam enantiomers binding to poly(SULL).

	Pocket 1	Pocket 2	Pocket 3	Pocket 4	Pocket 5	Pocket 6
R-Chlorthalidone						
$\Delta G_{binding}$ (kJ.mol^{-1})	−75.9	−59.5	−44.2	−86.0	−53.1	−42.1
Fraction occupied	0.02	–	–	0.98	–	–
% SASA decrease	71.1	66.3	48.9	77.2	51.9	48.7
		Pocket average $\Delta G_{binding} = -85.8$ kJ·mol^{-1}				
S-Chlorthalidone						
$\Delta G_{binding}$ (kJ.mol^{-1})	−96.0	−48.7	−111.0	−45.8	−41.3	−67.9
Fraction occupied	–	–	1.00	–	–	–
% SASA decrease	71.9	18.3	73.3	51.9	46.0	69.0
		Pocket average $\Delta G_{binding} = -111.01$ kJ·mol^{-1}				
R-Lorazepam						
$\Delta G_{binding}$ (kJ.mol^{-1})	−93.6	−52.4	−56.4	−62.1	−49.5	−58.3
Fraction occupied	1.00	–	–	–	–	–
% SASA decrease	71.4	42.2	44.8	46.4	46.5	40.9
		Pocket average $\Delta G_{binding} = -93.6$ kJ·mol^{-1}				
S-Lorazepam						
$\Delta G_{binding}$ (kJ.mol^{-1})	−71.6	−78.8	−70.9	−114.8	−103.1	−78.9
Fraction occupied	–	–	–	0.99	–	–
% SASA decrease	50.0	58.8	55.4	72.8	75.2	52.2
		Pocket average $\Delta G_{binding} = -114.7$ kJ·mol^{-1}				

poly(SULL) binding pockets. Figure 2 shows a representative plot of SASA versus simulation time for (R)-BOH binding to poly(SULL) pocket 6. A plot of SASA versus simulation time is also included for the MD simulation carried out with the ligand enantiomer in free solution. The arrow on the graph represents the percentage decrease in SASA.

The CPPTRAJ utilities in AMBER 14 were also used to investigate intermolecular hydrogen bond formation between ligand enantiomers and the MM dipeptide headgroups.[46] The criteria used to identify a hydrogen bond were as follows. The distance cutoff between the heavy atoms making up the hydrogen bond was 3.0 Å and the angle cutoff between the donor and acceptor atoms was ±30 °C.[46] These H-bond cutoffs are the default values in the AMBER 14 ccptraj utility and were also used in our previous MD simulation analyses.[24–28] Supplemental Tables S1–S5 present the hydrogen bond analyses carried out for each ligand enantiomer in the six poly(SULL) binding pockets. For each H-bond, the donor atom, acceptor atom, and percentage occupancy are reported. The later quantity corresponds to the percentage of the 60.0 ns simulation time that a given hydrogen bond was present.

Results and discussion

Poly(SULL) binding sites or pockets were identified as described above by first importing a representative poly(SULL) structure into the software package *MOE*. The software's site finder feature then identified the six distinct binding pockets shown in Figure 3a–3f.[40] In Figure 3, each

pocket is displayed as a solid surface with green and red colors corresponding to pocket regions that are, respectively hydrophobic or hydrophilic. Alpha spheres are also shown within each binding site. Red and white alpha spheres identify, respectively, good and poor hydrogen bonding locations within the pocket.[40–42] In other words, a pocket colored green and containing a large number of white alpha spheres is very hydrophobic, whereas a pocket colored red containing a large number of red alpha spheres is instead hydrophilic.

It should also be noted that the pockets shown in Figure 3a–3f are those found in a representative structure extracted from an MD simulation of the poly(SULL) MM. The monomer chains in the MM though are dynamic, so we would expect the exact nature of these pockets to fluctuate over time. However, the number of pockets and their diversity is governed by the number of monomers in the MM and the amino acids making up the dipeptide headgroup. So although the pocket properties may fluctuate as the chains move, the number and diversity of binding sites will likely remain largely the same. In other words, the pockets shown in Figure 3 represent a reasonable representation of the binding sites available to chiral compounds when they bind to poly(SULL).

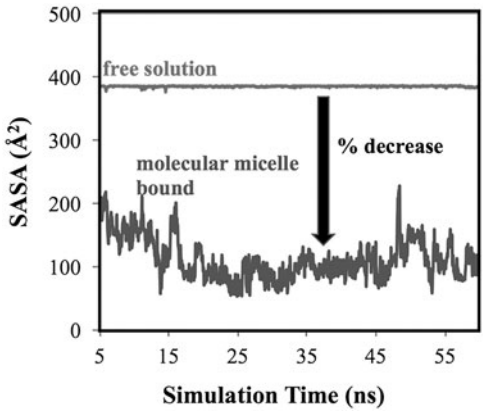

Figure 2. Plot of solvent-accessible surface area versus simulation time for (R)-BOH: pocket 6 MD simulation. The red and blue lines correspond to, respectively, a BOH MD simulation in free solution and bound to poly(SULL).

An examination of the poly(SULL) pockets in Figure 3 illustrates interesting differences between the binding sites formed by poly(SULL) and those detected in our previous work with the MM poly-(sodium undecyl-(L)-leucine-valine) or poly(SULV). First, poly(SULL) was found to form six binding pockets, compared to only four pockets found in poly(SULV).[26–28] More significantly, though the poly(SULL) analyses suggest that four of the MM's six binding sites, namely pockets 1–4 shown in Figure 3a–3d, are similar in both size and shape. This behavior contrasts previously reported behavior for poly(SULV) where a deep narrow pocket, two more non-polar dish-shaped pockets, and a fourth non-polar pocket near the MM surface were detected.[28] Figure 3a–3d suggest that poly(SULL) pockets 1–4 have similar electrostatic properties as well. This similarity is evident if we examine the number of white and red (i.e. hydrophobic or hydrophilic) alpha spheres placed by the *MOE* software in poly(SULL) pockets 1 (21 white and 4 red), 2 (27 white and 5 red), 3 (14 white and 6 red), and 4 (15 white and 3 red). This behavior is somewhat expected because poly(SULL) has two identical leucine amino acids in its dipeptide headgroup. Therefore, we might expect the biding pockets formed in different regions of poly(SULL) to be

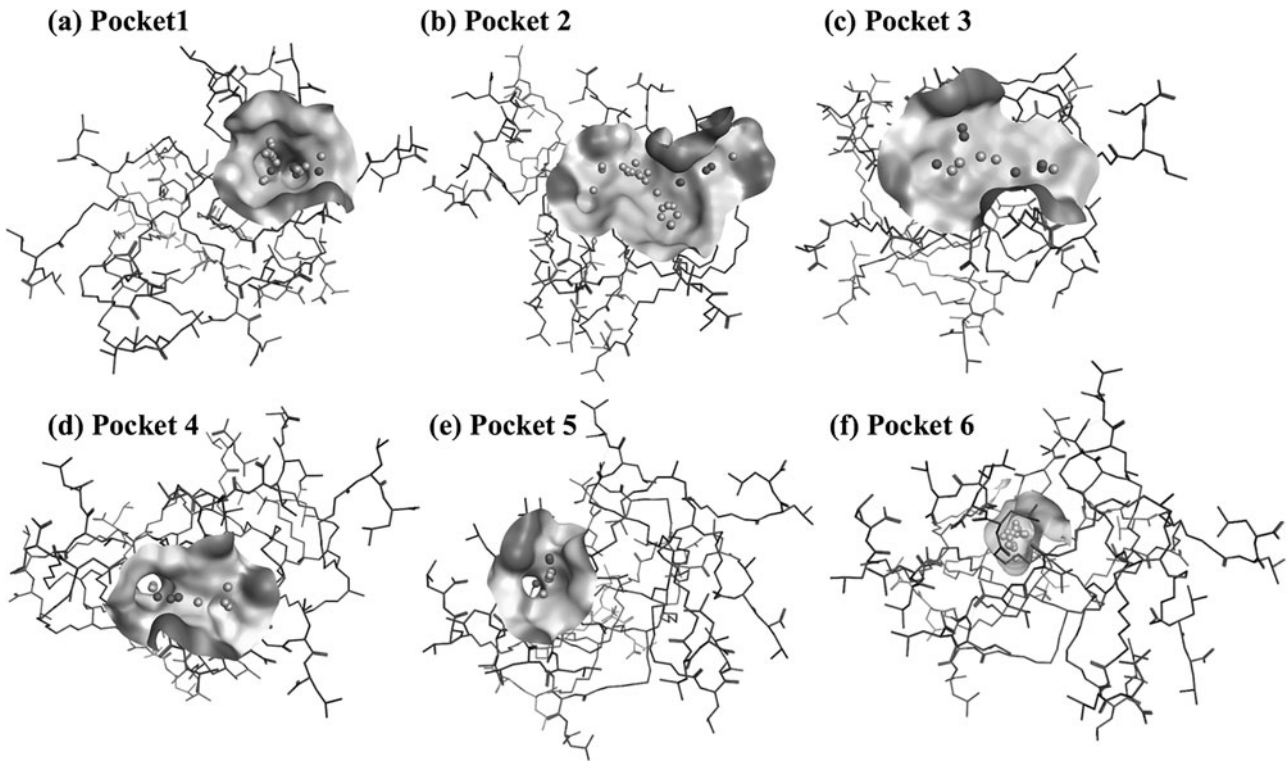

Figure 3. Poly(SULL) binding pockets. Green and red correspond to, respectively, hydrophobic and hydrophilic pocket regions.

similar as well. Furthermore, the poly(SULL) pockets shown in Figure 3 when compared to the poly(SULV) pockets reported in reference[28] suggest that changing the amino acids making up the dipeptide headgroup also changes the character of the MM's binding pockets.

Finally, poly(SULL) pockets 5 and 6 appear to be somewhat different than pockets 1–4. Figure 3e shows that poly(SULL) pocket 5 is primarily hydrophilic in nature with five red and only one white alpha spheres. Pocket 5, though, appears to be approximately the same size as poly(SULL) pockets 1–4. Finally, poly(SULL) pocket 6 is somewhat smaller than the other five pockets and is primarily hydrophobic in nature, with 28 white and no red alpha spheres. Also note that all of pocket 6 in Figure 3f is colored green further illustrating its non-polar nature.

We now move to an examination of how the chiral compounds listed above interact with these six poly(SULL) binding pockets. Results from the MD simulations with alprenolol:poly(SULL) intermolecular complexes are summarized in Table 1 and Supplemental Table S1. Table 1 gives free energies of MM binding, $\Delta G_{binding}$, and fractional occupancies, f_i, for (R) and (S)-alprenolol binding to poly(SULL) pockets 1 through 6. The pocket averaged $\Delta G_{binding}$ values in Table 1 for the (R) and (S) enantiomers of alprenolol were found to be −74.0 and −107.0 $kJ \cdot mol^{-1}$, respectively. Therefore, the MD simulation analyses predict that (S)-alprenolol interacts more favorably with poly(SULL) than (R)-alprenolol. This result is consistent with experiment, in that a CE analysis of a racemic alprenolol mixture using poly(SULL) as the chiral selector showed that (S)-alprenolol eluted after (R)-alprenolol.[22] Enantiomers separate in chiral CE based upon their relative free energies of binding to the chiral selector.[34–36] Therefore, the experimental CE results also show that (S)-alprenolol interacts with poly(SULL) more favorably that (R)-alprenolol.

Table 1 also shows that the binding free energy for both alprenolol enantiomers is lowest in poly(SULL) pocket 3. In (R)-alprenolol, the pocket 3 $f_i = 0.55$. This f_i value is the highest of the six pockets, however, pockets 2 and 6 have f_i values of 0.21 and 0.17, respectively. This result suggests that (R)-alprenolol can interact favorably with these poly(SULL) pockets as well. In contrast, the (S)-alprenolol pocket 3 f_i value is 0.93 indicating that the (S) enantiomer binds most strongly to this single MM pocket. Finally, for both alprenolol enantiomers, pocket 3 is likely preferred because alprenolol is a bulky, awkwardly shaped ligand and Figure 3 shows that pocket 3 is the largest of the six binding sites.

SASA analyses can be used to further rationalize why the alprenolol enantiomers have a high affinity for poly(SULL) pocket 3. For example, in the (R)-alprenolol pocket 3 MD simulation, the SASA percentage decrease in moving from free solution to the MM bound state was found to be 54.7%. This value represented the largest decrease among the six poly(SULL) binding pockets. In the (S)-alprenolol pocket 3 MD simulation, the corresponding SASA decrease was found to be 69.9%, which was also the largest decrease observed for the (S)-enantiomer. Therefore, the results of Table 1 show a correlation between a poly(SULL) pocket's free energy of ligand binding and the SASA decrease experienced by a ligand binding in that pocket, with the lowest $\Delta G_{binding}$ corresponding to a high SASA decrease. This result suggests that the alprenolol enantiomers bind preferentially to the poly(SULL) pocket that most effectively shields their hydrophobic atoms from solvent.

Supplemental Table S1 presents an analysis of the intermolecular hydrogen bonds formed during the alprenolol:poly(SULL) MD simulations. For each MM pocket, the percentage occupancies are listed for intermolecular hydrogen bonds that were present for more than 10% of the MD simulation time. The H-bond donor and acceptor atoms are given as well. In Supplemental Table S1, C-Leu and N-Leu are used to represent atoms on, respectively the C-terminal and N-terminal amino acids of the poly(SULL) dipeptide headgroup. The symbol C = O represents the carbonyl oxygen connecting the dipeptide headgroup to the surfactant monomer's hydrocarbon chain. Finally, recall that the poly(SULL) MM contained 19 covalently bound surfactant monomers. The surfactant monomer chain containing the atoms forming each hydrogen bond (identified as chains 1–19) are listed in Supplemental Table S1 as well.

The Supplemental Table S1 results show that the MM pocket with the lowest binding free energy is not necessarily the pocket where the most intermolecular hydrogen bonds formed between poly(SULL) and the alprenolol enantiomers. For example, (R)-alprenaolol had the lowest binding free energy in pocket 3, yet the intermolecular hydrogen bond percentage occupancies were actually higher in poly(SULL) pockets 2 and 5. (S)-alprenolol also had the lowest $\Delta G_{binding}$ in pocket 3, yet the percentage occupancies of the intermolecular H-bonds were higher in pocket 6. Therefore, the MD simulation results suggest that alprenolol enantiomers bind to the pocket that best shields their hydrophobic atoms from solvent (thus the large SASA decrease discussed above), but not necessarily to the pocket where ligand:MM hydrogen bonding is the strongest.

While hydrogen bonding interactions may not govern the preferred ligand binding site, the Supplemental Table S1 results suggest that the formation of intermolecular hydrogen bonds is an important factor in determining whether (R) or (S)-alprenolol interacts more strongly with the MM. Table 1 results show that both alprenolol enantiomers interact most favorably with poly(SULL) pocket 3. $\Delta G_{binding}$ of (S)-alprenolol, however, in pocket 3 is lower than the corresponding value for (R)-alprenolol in the same pocket. Examination of the Supplemental Table S1 results shows that in pocket 3, (S)-alprenolol forms seven intermolecular hydrogen bonds with poly(SULL) having percentage occupancies greater than 10%. The three highest occupancy (S)-alprenolol:poly(SULL) pocket 3 hydrogen bonds have percentage occupancies of 34.65%, 24.30%, and 21.04%. In contrast, (R)-alprenolol in pocket 3 forms only three hydrogen bonds with occupancies greater than 10%, the highest of which is 13.29%. The (R)-alprenolol f_i values in Table 1 show that the (R) enantiomer also has affinity for poly(SULL) pockets 2 and 6. However, the percentage occupancies of the (S)-alprenolol H-bonds in pocket 3 are generally larger than the corresponding (R)-alprenolol pocket 2

and 6 occupancies. Therefore, the alprenolol results suggest that once the ligand binds to the MM in its preferred low free energy pocket or pockets, the formation of stereoselective hydrogen bonds, that is, H-bonds that are different for the (R) and (S) enantiomers, plays an important role in governing whether the (R) or (S) enantiomer has the overall lowest binding free energy. Formation of these stereoselective hydrogen bonds would, therefore, be expected to determine the enantiomer's elution order in chiral CE separations as well, since elution order is determined by the relative free energies of MM binding for each of the ligand enantiomers.

Conclusions similar to those discussed above can also be drawn from the propranolol:poly(SULL) MD simulation analyses. Table 1 shows that the pocket-averaged MM binding free energy for (S)-propranolol is lower than the corresponding (R)-propranolol value. This result indicates that the (S) enantiomer experiences more favorable interactions with the MM and is consistent with experiment in that (S)-propranolol was found to elute after (R)-propranolol in CE separations with poly(SULL) as the chiral selector.[22] Table 1 also shows that (R)-propranolol had the lowest binding free energy in pocket 2, while $\Delta G_{binding}$ was lowest for (S)-propranolol in pocket 4. The f_i values were 1.00 for (R)-propranolol in pocket 2 and 0.95 for (S)-propranolol in pocket 4, suggesting that both propranolol enantiomers bind preferentially to a single poly(SULL) pocket. Furthermore, Figure 3 shows that poly(SULL) pockets 2 and 4 are very similar in size, shape, and electrostatic properties; therefore, it may not be surprising that the propranolol enantiomers do not necessarily prefer the same binding site.

As with alprenolol, the propranolol MD simulation analyses show that the decrease in ligand SASA upon moving from free solution to the MM-bound state is a good predictor of which MM pocket has the lowest $\Delta G_{binding}$ value. The SASA decrease of 52.3% for (R)-propranolol in pocket 2 was the second highest of the six pockets investigated and the SASA decrease of 67.4% for (S)-propranolol in pocket 4 was the largest decrease observed in the (S) enantiomer analyses. Therefore, both β-blockers (alprenolol and propranolol) preferentially bind to a MM pocket that effectively shields their hydrophobic rings from solvent.

In addition, once bound to the MM in the pocket with the lowest $\Delta G_{binding}$ and highest f_i values, the propranolol MD simulations suggest that hydrogen bond formation between the MM and propranolol enantiomers plays an important role in determining which enantiomer experiences the most favorable interactions with poly(SULL). Supplemental Table S2 shows that (S)-propranolol in pocket 4 forms seven hydrogen bonds with percentage occupancies greater than 10%; the highest being 46.63% between a terminal carboxylate oxygen atom of poly(SULL) monomer chain six and the (S)-propranolol hydroxyl hydrogen atom. In contrast, (R)-propranolol in pocket 2 forms five hydrogen bonds with occupancies greater than 10% with the highest value of only 21.53%. Therefore, as in the alprenolol MD simulation analysis, stereoselective hydrogen bond formation between the propranolol enantiomers and poly(SULL) likely plays an important role in determining chiral discrimination and elution order in CE experiments.

We will now consider the BOH and BNP MD simulation analyses. These compounds were investigated in part because their interactions with poly(SULL) have been studied experimentally.[22] Furthermore, these two binaphthyl compounds have very different structures than the β-blockers alprenolol and propranolol. Therefore, comparing the β-blocker and BOH/BNP results will allow us to assess whether the conclusions drawn above hold only for β-blockers and molecules with similar structures or if they apply more generally to a broader range of structurally diverse compounds. Table 2 shows that both enantiomers of BOH preferentially bind to MM pocket 6. The f_i values are 1.00 for both enantiomers in this pocket, indicating that the BOH enantiomers have a very high affinity for pocket 6 and a rather low affinity for the other poly(SULL) binding sites. In contrast, both enantiomers of BNP preferentially bind to poly(SULL) pocket 3 where the f_i values were 0.97 and 0.98 for (R)-BNP and (S)-BNP, respectively. These results can be rationalized based upon the shapes and electrostatic properties of the binaphthyl compounds and their preferred poly(SULL) binding pockets. Recall, pocket 6 is the most hydrophobic of the six poly(SULL) binding sites, containing 28 white/non-polar and no red or polar alpha spheres. Therefore, it seems reasonable that enantiomers of a non-polar molecule like BOH would have affinity for this pocket. BNP on the other hand is anionic and more polar than BOH. Its enantiomers, therefore, interact more favorably with pocket 3 which is more hydrophilic in nature than pocket 6. In fact, Figure 3 shows that with 14 white and 8 red alpha spheres, MM pocket 3 is among the most polar or hydrophilic poly(SULL) binding site.

The pocket averaged MM binding free energies for (R)-BOH and (S)-BOH are −88.1 and −61.6 $kJ \cdot mol^{-1}$, respectively. This result shows that unlike the β-blockers, the (R) enantiomer of BOH interacts more favorably with poly(SULL) than the (S) enantiomer. This result, however, is consistent with experiment because a CE separation of a racemic BOH mixture with poly(SULL) as the chiral selector showed that (R)-BOH eluted after (S)-BOH.[22] The pocket averaged $\Delta G_{binding}$ values for (R)-BNP and (S)-BNP are −45.7 and −66.4 $kJ \cdot mol^{-1}$, respectively. Again this result is consistent with experiment because in a CE separation of racemic BNP using poly(SULL) as the chiral selector, (S)-BNP eluted after (R)-BNP.[22] It also interesting to note that the association of the BOH enantiomers with poly(SULL) ($\Delta G_{binding} = -88.1$ and −61.6 $kJ \cdot mol^{-1}$ for the two enantiomers) is overall stronger than that of the corresponding BNP enantiomers ($\Delta G_{binding} = -45.7$ and −66.4 $kJ \cdot mol^{-1}$). This observation likely results from the more non-polar BOH enantiomers having a greater affinity for poly(SULL) which also has two non-polar leucine amino acids in its dipeptide headgroups. The binaphthyl compounds also interact less strongly with poly(SULL) than the β-blocker enantiomers. Again this result is expected given that the β-blockers are cationic and are thus attracted to the anionic MM. Alprenolol and propranolol also contain more hydrogen bond donor and acceptor atoms and thus likely form more hydrogen bonds with the poly(SULL) headgroups than BNP and BOH. Finally, NMR measurements of MM

binding constants also showed that BNP interacted less favorably with a different MM (poly(SULV)) than BOH, which in turn bound to the MM less strongly that propranolol.[47]

The MD simulations also suggest that both binaphthyl compounds bind to the pocket that best shields their fused rings from solvent. Furthermore, the formation of stereoselective hydrogen bonds between the binaphthyl compounds and MM headgoup atoms governs which BOH or BNP enantiomer has the lower $\Delta G_{binding}$. The former conclusion can be drawn by examining the percentage decrease in SASA upon moving from free solution to the MM-bound state. These values are given in Table 2 for both BOH and BNP. In the BOH MD simulations, pocket 6 was the MM binding site with the largest decrease in SASA, with values of 69.5% and 59.1% for (R)-BOH and (S)-BOH, respectively. Recall both enantiomers also had the lowest $\Delta G_{binding}$ in pocket 6. Both BNP enantiomers showed the largest decrease in SASA in pocket 3 (57.1% and 77.7% for (R)-BNP and (S)-BNP, respectively) which was also the pocket with the lowest free energy of MM binding for both enantiomers. Therefore, like the β-blockers BOH and BNP prefer binding to pockets that allow their enantiomers to penetrate into the MM core and shield their non-polar atoms from solvent exposure. Finally, it is also interesting to note that the SASA percentage decrease for (S)-BNP inserting into poly(SULL) pocket 3 was higher than the corresponding (R)-BNP value. This result suggests that (S)-BNP on average penetrates deeper into the MM hydrocarbon core than (R)-BNP. An analogous result was found in a previous MD simulation study of BNP binding to a different MM where(S)-BNP was also found to be more shielded from solvent than (R)-BNP in the MM bound state.[26]

The β-blocker and BOH/BNP results are also similar in that the MD simulations suggest that formation of stereoselective hydrogen bonds between the binaphthyl compounds and the MM headgroups plays an important role in governing which BOH or BNP enantiomer has the lower $\Delta G_{binding}$. The results of the BOH and BNP hydrogen bond analyses are shown in Supplemental Table S3. (R)-BOH in MM pocket 6, that is, the pocket with the lowest $\Delta G_{binding}$, formed four hydrogen bonds with occupancies greater than 10%. The highest occupancy hydrogen bond was 48.01% between a terminal carboxylate oxygen atom on poly(SULL) chain 12 and an (R)-BOH hydroxyl hydrogen atom. In contrast, (S)-BOH in pocket 6 formed only one high occupancy intermolecular hydrogen bond (24.74%). Similarly, (S)-BNP had a lower $\Delta G_{binding}$ than (R)-BNP and in pocket 3 the (S) enantiomer formed hydrogen bonds with occupancies of 19.66%, 16.21%, and 12.19% between BNP oxygen atoms and NH donor atoms on the poly(SULL) headgroups. (R)-BNP in contrast, formed only two intermolecular hydrogen bonds (13.44% and 12.05% occupancies) with the poly(SULL) headgroup atoms.

Therefore, it can be concluded that even though the β-blockers and binaphthyl compounds have very different structures, they exhibit similar behavior when binding to poly(SULL). The MD simulations suggest that enantiomers of all four compounds (alprenolol, propranolol, BOH, and BNP) interact preferentially with MM binding pockets that effectively shield their hydrophobic-fused rings from the solvent. Within this preferred pocket, the ligand enantiomer experiencing the larger number or more favorable hydrogen bonding interactions with the MM has the lower $\Delta G_{binding}$ value and would be expected to elute last in a chiral CE separation. We will now investigate whether this same binding model can be applied to the chiral drugs chlorthalidone and lorazepam.

Table 3 shows that pocket-averaged $\Delta G_{binding}$ for (S)-chlorthalidone and (S)-lorazepam are lower than the corresponding values for the (R) enantiomers of both compounds. To the best of our knowledge, the chiral CE elution order of chlorthalidone and lorazepam enantiomers has not been reported, so the results of these free energy calculations cannot be compared to experiment. However, MD simulations from the literature showed that the (S) enantiomers of both compounds had lower pocket-averaged $\Delta G_{binding}$ values when they bound to the MM poly(SULV).[28] Therefore, the poly(SULL) free energy of binding results presented here are consistent with these literature results.

Table 3 also shows that as in the β-blocker, BOH, and BNP analyses, enantiomers of chlorthalidone and lorazepam bind preferentially to poly(SULL) binding pockets where there is a large percentage decrease in the ligand SASA when moving between free solution to the MM-bound states. In other words, chlorthalidone and lorazepam enantiomers prefer poly(SULL) pockets that allow the ligands to penetrate into the MM hydrocarbon core where they are shielded from solvent exposure. For example, (R)-chlorthalidone was found to interact most favorably with poly(SULL) pocket 4 ($\Delta G_{binding} = -86.0\,kJ{\cdot}mol^{-1}$, $f_i = 0.98$) where the SASA decrease was 77.2%. $\Delta G_{binding}$ for (S)-chlorthalidone was lowest in pocket 3 ($\Delta G_{binding} = -111.0\,kJ{\cdot}mol^{-1}$ and $f_i = 1.00$) where the SASA decrease was also high (73.3%). The lorazepam MD simulation results are similar, with (R)-lorazepam in pocket 1 having $\Delta G_{binding} = -93.6\,kJ{\cdot}mol^{-1}$, an f_i value of 1, and a corresponding SASA decrease of 71.4%. (S)-lorazepam in pocket 4 had $\Delta G_{binding} = -114.8\,kJ{\cdot}mol^{-1}$, $f_i = 0.99$, and an SASA decrease of 72.8%. Again with both enantiomers, the MM pockets with the most favorable free energies of enantiomer binding also effectively shielded the lorazepam enantiomers from solvent exposure. Finally, it should also be noted that like propranolol, the chlorthalidone and lorazepam enantiomer had their lowest $\Delta G_{binding}$ values in different poly(SULL) binding pockets. However, this result may be rationalized based upon the similarity in size, shape, and electrostatic properties of poly(SULL) pockets 1–4 (see Figure 2).

As with the β-blockers, BOH, and BNP, the chlorthalidone MD simulation results suggest that stereoselective hydrogen bond formation contributes to (S)-chlorthalidone having a lower pocket averaged $\Delta G_{binding}$ than (R)-chlorthalidone. (R)-chlorthalidone binds preferentially to pocket 4 where the results presented in Supplemental Table S4 show that three intermolecular hydrogen bonds with occupancies of 30.66%, 13.18%, and 12.67% were detected. (S)-chlorthalidone in contrast, binds most strongly to SULL pocket 3 where six high-occupancy intermolecular hydrogen bonds

were formed, three of which were over 30%. Therefore, with chlorthalidone we see that the enantiomer with the lowest $\Delta G_{binding}$ also experiences more favorable hydrogen bonding interactions with the MM.

The results of the lorazepam:poly(SULL) hydrogen bonding analysis shown in Supplemental Table S5, however, are less straightforward. (R)-lorazepam was found to bind preferentially to poly(SULL) pocket 1 where Supplemental Table S5 shows that two intermolecular hydrogen bonds with occupancies of 42.16% and 18.01% were detected. (S)-lorazepam bound most strongly to poly(SULL) pocket 4 where there were more intermolecular hydrogen bonds (four versus two for (R)-lorazepam), but the percentage occupancies of these hydrogen bonds were generally lower (21.82%, 18.08%, 16.80%, and 14.01%). Therefore, we cannot conclude that (S)-lorazepam has the lower free energy of poly(SULL) binding simply because the (S) enantiomer has more favorable hydrogen bonding interactions with the MM.

A previous investigation of lorazepam binding to a different MM (poly(SULV)) showed that ligand penetration into the MM hydrocarbon core, intermolecular hydrogen bonding, and the orientation adopted by the ligand enantiomers within each pocket were all important factors in determining how strongly each enantiomer interacted with the MM.[28] The lorazepam enantiomers were found to interact most favorably with the MM pockets when the molecule's seven-membered and two aromatic rings were all oriented toward the MM hydrocarbon core. Less favorable orientations of the rings with respect to the hydrocarbon core and solvent phase lead to less favorable $\Delta G_{binding}$ values.[28] Similar behavior may be occurring in the lorazepam:poly(SULL) system. A more detailed analysis of all the factors governing the binding of lorazepam enantiomers to poly(SULL) is currently underway.

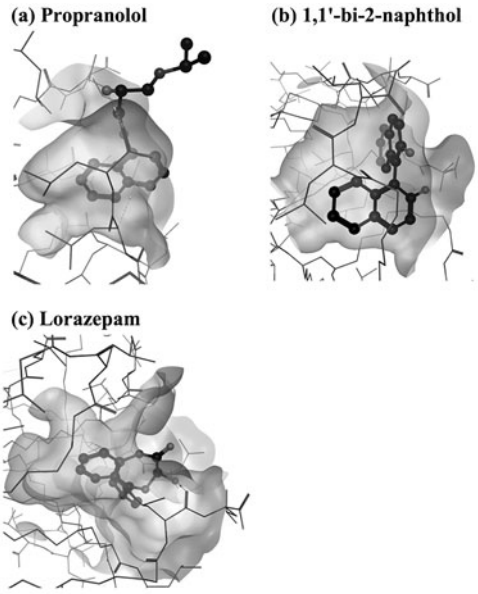

Figure 4. Structures extracted from MD simulations showing ligands inserted into micelle core. (a) (S)-propranolol:poly(SULL) complex at 21.8 ns, (b) (R)-BOH:poly(SULL) complex at 41.0 ns, and (c) (S)-lorazepam:poly(SULL) complex at 19.0 ns.

Finally, one conclusion drawn from all of the above MD simulation results is that the ligands investigated bind preferentially to a poly(SULL) pocket that shielded their hydrophobic rings from solvent exposure. Figure 4 shows three representative structures extracted from the MD simulations that show ligand enantiomers inserted into the binding pockets in this manner. Figure 4a shows a structure extracted from the (S)-propranolol: pocket 4 MD simulation at 21.8 ns. Figure 4b shows a structure extracted from the (R)-BOH: pocket 6 MD simulation at 41.0 ns, and Figure 4c is a structure extracted from the (S)-lorazepam: pocket 4 MD simulation at 19.0 ns. The structures at each of these time steps were found to have a low RMSD value with respect to the average structure. As shown in Figure 3, the polar and non-polar regions of the Figure 4 binding pockets are colored red and green, respectively. Each of the Figure 4 structures shows the ligands' hydrophobic fused rings pointing into the non-polar pocket region and oriented toward the poly(SULL) hydrocarbon core.

Conclusions

MD simulations have been used to investigate the stereoselective binding of six different chiral compounds to the amino acid-based MM poly(SULL). Poly(SULL) was found to have six pockets or binding sites into which chiral ligand enantiomers could insert. Four of these pockets were found to have similar sizes, shapes, and electrostatic properties. All six chiral compounds bound most strongly to a poly(SULL) pocket that shielded their non-polar atoms from solvent. In five of the six compounds studied, the formation of stereoselective intermolecular hydrogen bonds determined which enantiomer had the lower free energy of MM association. This enantiomer would be expected to elute last in a chiral CE separation. Subsequent studies will further test this model with single amino acid and other dipeptide MM before using the model to develop molecular modeling-based techniques that will identify the best MM for a given chiral separation problem.

Acknowledgments

This work was supported by an NIH-NIMHD grant (#G12 MD007579) to the RCMI Program at Howard University, NSF-RUI grants (#1709680, #1709394, and #1708959), a Robert A. Welch Chemistry Departmental Grant to the Chemistry Program at Texas A&M University-Corpus Christi, an NSF CAREER grant (#0449742) to Dr. Eugene Billiot and a HUMAA Endowed Founder's Chair in Basic Science award and Office of Naval Research grants (#N00014-17-1-2105 and #N00014-18-2145) grants to Dr. Yayin Fang. We also acknowledge the generosity of the Ralph E. Klingenmeyer family.

References

[1] Li, B.; Haynie, D. T. Chiral Drug Separation. *Encycl. Chem. Process*. **2016**, *1*, 449–458.
[2] Lin, G.; You, Q.; Cheng, J. *Chiral Drugs: Chemistry and Biological Action*; Wiley & Sons: Hoboken, NJ, **2011**.

[3] Announcement. FDA's Policy Statement for the Development of New Stereoisomeric Drugs. *Chirality*. **1992**, *4*, 338.

[4] Subramanian, G. *Chiral Separation Techniques*, 3rd ed.; Wiley-VCH: New York, **2007**.

[5] Ward, T. J.; Ward, K. D. Chiral Separations: Fundamental Review 2010. *Anal. Chem*. **2010**, *82*, 4712–4722.

[6] Valle, B. C.; Morris, K. F.; Fletcher, K. A.; Fernand, V.; Sword, D. M.; Eldridge, S.; Larive, C. K.; Warner, I. M. Understanding Chiral Molecular Micelle Separations Using Steady-State Fluorescence Anisotropy, Capillary Electrophoresis, and NMR. *Langmuir*. **2007**, *23*, 425–435.

[7] Sciba, G. K. E. Chiral Recognition in Separation Science – An Update. *J. Chromatogr. A*. **2016**, *1467*, 56–78.

[8] Billiot, E. J.; Macossay, J.; Thibodeaux, S.; Shamsi, S. A.; Warner, I. M. Chiral Separations Using Dipeptide Polymerized Surfactants: Effect of Amino Acid Order. *Anal. Chem*. **1998**, *70*, 1375–1381.

[9] Wang, J.; Warner, I. M. Chiral Separations Using Micellar Electrokinetic Chromatography and a Polymerized Chiral Micelle. *Anal. Chem*. **1994**, *66*, 3773–3776.

[10] Dobashi, A.; Hamada, M.; Dobashi, Y.; Yamaguchi, J. Enantiomeric Separation with Sodium Dodecanoyl-L-Amino Acidate Micelles and Poly(Sodium (10-Undecenoyl)-L-Valinate) by Electrokinetic Chromatography. *Anal. Chem*. **1995**, *67*, 3011–3017.

[11] Palmer, C. P. Micelle Polymers, Polymer Surfactants, and Dendrimers as Pseudostationary Phases in Micellar Electrokinetic Chromatography. *J. Chromatogr. A*. **1997**, *780*, 75–92.

[12] Billiot, E. J.; Warner, I. M. Examination of Structural Changes of Polymeric Amino Acid-Based Surfactants on Enantioselectivity: Effect of Amino Acid Order, Steric Factors, and Number and Position of Chiral Centers. *Anal. Chem*. **2000**, *72*, 1740–1748.

[13] Billiot, E. J.; Agbaria, R.; Thibodeaux, S.; Shamsi, S. A.; Warner, I. M. Amino Acid Order in Dipeptide Surfactants: Effect on Physical Properties and Enantioselectivity. *Anal. Chem*. **1999**, *71*, 1252–1256.

[14] Shamsi, S. A.; Warner, I. M. Monomeric and Polymeric Chiral Surfactants as Pseudostationary Phases for Chiral Separations. *Electrophoresis* **1997**, *18*, 853–872.

[15] Haddadian, F. H.; Shamsi, S. A.; Warner, I. M. Chiral Electrokinetic Chromatography Using Dipeptide Polymeric Surfactants: State of the Art. *Electrophoresis*. **1999**, *20*, 3011–3026.

[16] Hayes, J. L.; III.; Warner, I. M. Polymeric Surfactants as Pseudostationary Phases for Separations in Electrokinetic Chromatography (EKC): A Review. *Rev. Anal. Chem*. **1999**, *18*, 317–382.

[17] Yarabe, H. H.; Billiot, E. J.; Warner, I. M. Enantiomeric Separations by Use of Polymeric Surfactant Electrokinetic Chromatography. *J. Chromatogr. A*. **2000**, *875*, 179–206.

[18] Haynes, I. I. I.; J. L.; Billiot, E. J.; Yarabe, H. H.; Shamsi, S. A.; Warner, I. M. Chiral Separations with Dipeptide-Terminated Polymeric Surfactants: The Effect of an Extra Hetroatom on the Polar Head Group. *Electrophoresis*. **2000**, *21*, 1597–1605.

[19] Thibodeaux, S. J.; Billiot, E. J.; Torres, E.; Valle, B. C.; Warner, I. M. Enantiomeric Separations Using Polymeric L-Glutamate Surfactant Derivatives: Effect of Increasing Steric Factors. *Electrophoresis*. **2003**, *24*, 1077–1082.

[20] Billiot, F. H.; Billiot, E. J.; Warner, I. M. Depth of Penetration of Binaphthyl Derivatives into the Micellar Core of Sodium Undecenoyl Leucyl-Leucinate Surfactants. *J. Chromatogr. A*. **2002**, *950*, 233–239.

[21] Shamsi, S. A.; Valle, B. C.; Billiot, F.; Warner, I. M. Polysodium *N*-Undecanoyl-L-Leucylvalinate: A Versatile Chiral Selector for Micellar Electrokinetic Chromatography. *Anal. Chem*. **2003**, *75*, 379–387.

[22] Billiot, E. J.; Thibodeaux, S.; Shamsi, S. A.; Warner, I. M. Evaluating Chiral Separation Interactions by Use of Diastereometric Polymeric Dipeptide Surfactants. *Anal. Chem*. **1999**, *71*, 4044–4049.

[23] Haddadian Billiot, F.; McCarroll, M. E.; Billiot, E. J.; Rugutt, J. K.; Morris, K. F.; Warner, I. M. Comparison of the Aggregation Behavior of Fifteen Polymeric and Monomeric Dipeptide Surfactants in Aqueous Solution. *Langmuir*. **2002**, *18*, 2993–2997.

[24] Morris, K. F.; Billiot, E. J.; Billiot, F. H.; Lipkowitz, K. B.; Southerland, W. M.; Fang, Y. Investigation of Chiral Molecular Micelles by NMR Spectroscopy and Molecular Dynamics Simulations. *OJPC*. **2012**, *2*, 2, 240–251.

[25] Morris, K. F.; Billiot, E. J.; Billiot, F. H.; Lipkowitz, K. B.; Southerland, W. M.; Fang, Y. A Molecular Dynamics Simulation Study of Two Dipeptide-Based Molecular Micelles: Effect of Amino Acid Order. *OJPC*. **2013**, *3*, 20–29. 3,

[26] Morris, K. F.; Billiot, E. J.; Billiot, F. H.; Lipkowitz, K. B.; Southerland, W. M.; Gladis, A. A.; Fang, Y. A Molecular Dynamics Simulation Study of the Association of 1,1′-Binaphthyl-2,2′-Diyl Hydrogenphosphate Enantiomers with a Chiral Molecular Micelle. *Chem. Phys*. **2014**, *439*, 36–43.

[27] Morris, K. F.; Billiot, E. J.; Billiot, F. H.; Hoffman, C. B.; Gladis, A. A.; Lipkowitz, K. B.; Southerland, W. H.; Fang, Y. Molecular Dynamics Simulation and NMR Investigation of the Association of the *β*-Blockers Atenolol and Propranolol with a Chiral Molecular Micelle. *Chem. Phys*. **2015**, *457*, 133–146.

[28] Morris, K. F.; Billiot, E. J.; Billiot, F. H.; Ingle, J. A.; Zack, S. R.; Krause, K. B.; Lipkowitz, K. B.; Southerland, W. H.; Fang, Y. Investigation of Chiral Recognition by Molecular Micelles with Molecular Dynamics Simulations. *J. Dispersion Sci. Technol*. **2018**, *39*, 45–54.

[29] Chlorthalidone, U.S. National Library of Medicine: Medline Plus, **2013**.

[30] Marchand, A. P.; Chong, H. S.; Ganguly, B. Synthesis of a Novel Cage-Functionalized Chiral Binaphthol Host: A Potential New Agent for Enantioselective Recognition of Chiral Ammonium Salts. *Tetrahedr. Asym*. **1999**, *10*, 4695–4707.

[31] Jiehao, C.; Craig, J. F. Total Synthesis of Apratoxin A. *J. Am. Chem. Soc*. **2003**, *125*, 8734–8735.

[32] Billiot, F. H.; McCarroll, M. E.; Billiot, E. J.; Warner, I. M. Chiral Recognition of Binaphthyl Derivatives Using Electrokinetic Chromatography and Steady-State Fluorescence Anisotropy: Effect of Temperature. *Electrophoresis*. **2004**, *25*, 753–757.

[33] Rugutt, J. K.; Billiot, E. J.; Warner, I. M. NMR Study of the Interaction of Monomeric and Polymeric Chiral Surfactants with (R)- and (S)-1,1′-Binaphthyl-2,2′-Diyl Hydrogen Phosphate. *Langmuir*. **2000**, *16*, 3022–3029.

[34] Yarabe, H. H.; Rugutt, J. K.; McCarroll, M. E.; Warner, I. M. Capillary Electrophoretic Separation of Binaphthyl Enantiomers with Two Polymeric Chiral Surfactants: ^{1}H-Nuclear Magnetic Resonance and Fluorescence Spectroscopy Study. *Electrophoresis*. **2000**, *21*, 2025–2032.

[35] Kingsbury, S. A.; Ducommun, C. J.; Zahakaylo, B. M.; Dickinson, E. H.; Morris, K. F. NMR Characterization of 1,1′-Binaphthyl-2,2′-Diyl Hydrogen Phosphate Binding to Chiral Molecular Micelles. *Magn. Reson. Chem*. **2010**, *48*, 184–191.

[36] McCarroll, M. E.; Billiot, F. H.; Warner, I. M. Fluorescence Anisotropy as a Measure of Chiral Recognition. *J. Am. Chem. Soc*. **2001**, *123*, 3173–3174.

[37] Xu, Y.; McCarroll, M. E. Fluorescence Anisotropy as a Method to Examine the Thermodynamics of Enantioselectivity. *J Phys. Chem. B*. **2005**, *109*, 8144–8152.

[38] Lorazepam, U.S. National Library of Medicine: Medline Plus, **2010**.

[39] Case, D. A.; Babin, V.; Berryman, J. T.; Betz, R. M.; Cai, Q.; Cerutti, D. S.; Cheatham III, T. E.; Darden, T. A.; Duke, R. E.; Gohlke.; et al. *AMBER 14*. San Francisco: University of California, **2014**.

[40] Molecular Operating Environment (MOE), Chemical Computing Group, **2016**.

[41] Edelsbrunner, H.; Mucke, E. P. Three Dimensional Alpha Shapes. *ACM Trans. Graph*. **1994**, *13*, 43–72.
[42] Edelsbrunner, H.; Shah, N. R. Incremental Topological Flipping Works for Regular Triangulations. *Algorithmica*. **1996**, *15*, 223–241.
[43] Dal Ben, D.; Buccioni, M.; Lambertucci, C.; Thomas, A.; Volpini, R. Simulation and Comparative Analysis of Binding Modes of Nucleoside and Non-Nucleoside Agonists at the A_{2B} Adenosine Receptor. *In Silico Pharmacol*. **2013**, *1*, 24–38.
[44] Wang, J.; Cieplak, P.; Kollman, P. A. How Well Does a Restrained Electrostatic Potential (RESP) Model Perform in Calculating Conformational Energies of Organic and Biological Molecules? *J. Comput. Chem*. **2000**, *21*, 1049–1074.
[45] Kollman, P. A.; Massova, I.; Reyes, C.; Kuhn, B.; Huo, S.; Chong, L.; Lee, M.; Lee, T.; Duan, Y.; Wang, W.; et al. Calculating Structures and Free Energies of Complex Molecules: Combining Molecular Mechanics and Continuum Models. *Acc. Chem. Res*. **2000**, *33*, 889–897.
[46] Roe, D. R.; Cheatham, T. E. III, PTRAJ and CPPTRAJ: Software for Processing and Analysis of Molecular Dynamics Trajectory Data. *J. Chem. Theory Comput*. **2013**, *9*, 3084–3095.
[47] Morris, K. F.; Becker, B. A.; Valle, B. C.; Warner, I. M.; Larive, C. K. Use of NMR Binding Interaction Mapping Techniques to Examine Interactions of Chiral Molecules with Molecular Micelles. *J. Phys. Chem. B*. **2006**, *110*, 17359–17369.